Journal of Magnetic Resonance 212 (2011) 64–73

Contents lists available at ScienceDirect

Journal of Magnetic Resonance

journal homepage: www.elsevier.com/locate/jmr

Structure determination in "shiftless" solid state NMR of oriented protein samples

Yuanyuan Yin, Alexander A. Nevzorov *

Department of Chemistry, North Carolina State University, 2620 Yarbrough Drive, Raleigh, NC 27695-8204, USA

ARTICLE INFO

Article history:
Received 21 February 2011
Revised 9 June 2011
Available online 7 July 2011

Keywords:
"Shiftless" solid-state NMR
Dipolar couplings
Angular constraints
Non-planarity
Protein structure determination

ABSTRACT

An efficient formalism for calculating protein structures from oriented-sample NMR data in the torsion-angle space is presented. Angular anisotropies of the NMR observables are treated by utilizing an irreducible spherical basis of rotations. An intermediate rotational transformation is introduced that greatly speeds up structural fitting by rendering the dependence on the torsion angles Φ and Ψ in a purely diagonal form. Back-calculation of the simulated solid-state NMR spectra of protein G involving ^{15}N chemical shift anisotropy (CSA), and ^{1}H–^{15}N and $^{1}H_{\alpha}$–$^{13}C_{\alpha}$ dipolar couplings was performed by taking into account non-planarity of the peptide linkages and experimental uncertainty. Even a relatively small (to within 1 ppm) random variation in the CSA values arising from uncertainties in the tensor parameters yields the RMSD's of the back-calculated structures of more than 10 Å. Therefore, the ^{15}N CSA has been substituted with heteronuclear dipolar couplings which are derived from the highly conserved bond lengths and bond angles associated with the amino-acid covalent geometry. Using the additional $^{13}C_{\alpha}$–^{15}N and $^{13}C'$–^{15}N dipolar couplings makes it possible to calculate protein structures entirely from "shiftless" solid-state NMR data. With the simulated "experimental" uncertainty of 15 Hz for protein G and 120 Hz for a helical hairpin derived from bacteriorhodopsin, back-calculation of the synthetic dipolar NMR spectra yielded a converged set of solutions. The use of distance restraints dramatically improves structural convergence even if larger experimental uncertainties are assumed.

1. Introduction

In the past two decades, solid-state NMR of uniaxially aligned samples has been successfully applied to three-dimensional structure determination of membrane proteins [1–7]. Due to substantial improvements in the decoupling pulse sequences [8–12] and methods of alignment [13–15], oriented-sample NMR has demonstrated its effectiveness as a complementary method to traditional X-ray diffraction and solution and magic-angle spinning (MAS) NMR spectroscopy for studying membrane proteins.

In solid-state NMR of oriented samples, membrane proteins are aligned uniaxially in the phospholipid bilayer environment, so that the experimental observables are orientationally dependent, and the structural information is directly contained in the NMR spectra. The observables typically include heteronuclear dipolar couplings and chemical shift anisotropy (CSA) associated with the isotopically labeled ^{15}N or ^{13}C sites. Previously, protein backbone structures were determined by assembling the final structure from fragments of peptide planes by calculating the possible orientations of the magnetic field relative to the molecular frame associated with each residue [1,16,17]. The orientational degeneracies were reduced by examining the chemical and steric allowances as suggested by the Ramachandran plot, chemical shift values, the angles calculated from the dipole-dipole and quadrupolar interactions, and bond angles and distances between the specific atoms [1,16–18]. To improve resolution and reduce the degeneracy of the structural solutions, measurements involving the alpha carbon ($^{13}C_{\alpha}$), such as the chiral $^{1}H_{\alpha}$–$^{13}C_{\alpha}$ dipolar couplings, may need to be introduced [19] in addition to the most widely used ^{15}N CSA and ^{1}H–^{15}N dipolar couplings. New triple-resonance pulse sequences [20] involving ^{15}N and ^{13}C correlations and "shiftless" acquisition techniques [21] are especially encouraging in this regard.

So far, only the planar form of the *trans* peptide unit has been used as the standard geometry for structure calculations in oriented-sample NMR. However, back in 1968 Ramachandran pointed out the significance of out-of-plane distortions in the polypeptide chains, especially in cyclic peptides, which was supported by energy calculations [22,23]. A survey on the torsion angles ω describing the rotation around the amide bond in peptides and proteins was implemented by considering the Cambridge Structural Database (CSD) of small molecules and the Brookhaven Protein Databank (PDB), which showed that for all good-quality crystal structures, the average twist was around 0.5° [24]. Scheiner and Kern have indicated that certain environmental effects such as the formation of hydrogen bonds contributed to the non-planar conformation as well [25]. Consequently, out-of-plane deviations

* Corresponding author. Fax: +1 919 515 2545.
E-mail address: Alex_Nevzorov@ncsu.edu (A.A. Nevzorov).

1090-7807/$ - see front matter © 2011 Elsevier Inc. All rights reserved.
doi:10.1016/j.jmr.2011.06.008

of the peptide linkages should be included in the refinement of the calculated protein structures.

Another potential problem affecting the accuracy of the calculated structures is the possible variations in the magnitude of the principal components and orientation of the shielding tensor along the polypeptide chains [26,27]. A more recent work [28] provides a comprehensive review of the variation of CSA in soluble proteins. In a quantum mechanical study on the chemical shift tensors of peptides [29], the most shielded component of the ^{15}N chemical shift tensor was found to deviate substantially from the peptide plane particularly in helical domains, and the principal value of the $^{13}C_\alpha$ chemical shift tensor along the $^{1}H_\alpha$–$^{13}C_\alpha$ bond was found to be very sensitive to the torsion angles Φ and Ψ. In addition to the variations in the tensor values, there is also experimental accuracy (uncertainty) in the determination of the values themselves. Lee et al. [30] reported the ^{15}N chemical shift tensor parameters for the ^{15}N-Gly-18 residue to be $\sigma_{11N} = 42 \pm 2$ ppm, $\sigma_{22N} = 73 \pm 2$ ppm, $\sigma_{33N} = 215 \pm 2$ ppm, $\alpha_N = 30 \pm 10°$, $\beta_N = 22 \pm 2°$ (here, α_N and β_N describe the orientation of the chemical shift tensor relative to the molecular frame); whereas the parameters for ^{15}N-Phe-16 were $\sigma_{11N} = 55 \pm 2$ ppm, $\sigma_{22N} = 80 \pm 2$ ppm, $\sigma_{33N} = 220 \pm 2$ ppm, $\alpha_N = 45 \pm 15°$, $\beta_N = 22 \pm 3°$. These findings indicated a significant effect of the local chemical and geometrical environment on the magnitude and orientation of the ^{15}N CSA [31]. While the principal components of the CSA tensor can be directly measured for each specific amino-acid site of the protein using either the Herzfeld–Berger method [32] as in MAS NMR [33,34], or relaxation methods as in solution NMR [35], the orientation of the tensor relative to each peptide plane is somewhat less precisely determined.

Nonetheless, in structure calculations from oriented-sample NMR data, the ^{15}N CSA tensor is usually assumed to have the same orientation and average values of the principal components for all amino-acid residues: $\sigma_{11N} = 64$ ppm, $\sigma_{22N} = 77$ ppm, $\sigma_{33N} = 217$ ppm [36,37] (for glycines these values are assumed to be $\sigma_{11N} = 41$ ppm, $\sigma_{22N} = 64$ ppm, $\sigma_{33N} = 210$ ppm). For alpha-helical structures with the highly constrained torsion angles Φ and Ψ and well-defined hydrogen bonding, the above-mentioned tensor variations and uncertainties do not generally represent a problem since the arising orientational solutions can be easily sorted out [16–18,38–40]. Structures of macroscopically aligned proteins having up to 50 residues can be obtained even in the presence of short connecting loops by imposing weak packing and hydrophobic restraints [4]. However, the variations and/or uncertainty in the tensor parameters can become an important issue in calculating backbone conformations with less restrained torsion angles such as the connecting interhelical loops or β-type structures. This becomes evident from the fact that the orientational restraints (dipolar couplings, CSA) provide only one or two angles that define the orientation of the peptide plane relative to the laboratory frame; whereas *three* Euler angles are necessary to unequivocally define the orientation of a rigid body. Therefore, the calculated structures can branch off at a point where the multiple solutions corresponding to the relative orientations of the adjacent peptide units are distributed uniaxially around the main magnetic field. It has been shown [19] that in the absence of uncertainty in the tensor values and experimental error there is a mathematically unique structural solution to a three-dimensional solid-state NMR spectrum (including ^{15}N CSA, and ^{1}H–^{15}N and $^{1}H_\alpha$–$^{13}C_\alpha$ dipolar couplings). However, the above-mentioned uncertainties are still inevitably contained in the experimental data. In the present paper we evaluate the effect of experimental error on the accuracy and convergence of the calculated structures. Resolving these important issues could potentially give way to a complete *de novo* structure determination of membrane proteins of arbitrary topology as experimentally determined dipolar couplings for the doubly-labeled proteins become available.

2. NMR observables in the spherical basis and the algorithm

In oriented-sample (OS) NMR spectroscopy, the structural information is obtained directly from angular-dependent observables; therefore, the Cartesian basis is not very efficient. To deal with the constraints in the angular space and minimize the number of required calculations we choose the irreducible spherical basis of rank 1 to relate the protein structure to its multidimensional solid-state NMR spectra. The molecular frame (MF) depicted in Fig. 1 is associated with an individual peptide plane, in which the *x*-axis is along the NH bond, and the *z*-axis is perpendicular to the plane determined by the N–H and C′–N bonds (where C′ denotes the carbonyl atom). The orientation of the magnetic field B_0 relative to the MF is described by the angles α and β. To avoid explicit calculation of the trigonometric functions in the NMR frequencies, a more compact quadratic form was previously employed [19]:

$$\nu = \vec{\mathbf{Y}}(\beta,\alpha)[\mathbf{D}(\Omega_{MP})\mathbf{M}\mathbf{D}^{-1}(\Omega_{MP})]\vec{\mathbf{Y}}^{+}(\beta,\alpha) \quad (1)$$

Here $\vec{\mathbf{Y}}(\beta,\alpha)$ denotes the row vector of the unnormalized spherical harmonics, $\vec{\mathbf{Y}}(\beta,\alpha) = \left(-\frac{\sin\beta}{\sqrt{2}}e^{i\alpha} \quad \cos\beta \quad \frac{\sin\beta}{\sqrt{2}}e^{-i\alpha}\right)$. The rank-1 Wigner rotation matrix $\mathbf{D}(\Omega_{MP})$ describes the transformation from the MF to the principal axis system of each tensor, and the superscript "+" denotes the Hermitian conjugate. The matrix **M** corresponds to the specific type of interactions (e.g. CSA or dipolar) as defined below.

To include deviations from the planarity of peptide units, the following propagator matrix is introduced by employing a product of three Wigner rotation matrices:

$$\begin{aligned}\mathbf{P}(\Phi_n,\Psi_n,\omega_n) =& \mathbf{D}(\alpha_{NC_\alpha},\Phi_n,\gamma_{tetra})\mathbf{D}(0,-\Psi_n-\pi,0)\\ & \mathbf{D}(-\alpha_{NC'C_\alpha},\pi-\omega_n,-\pi/2-\gamma_{HNC'})\end{aligned} \quad (2)$$

The three torsion angles that result in the secondary and tertiary conformations of the polypeptide chains are denoted as Φ_n, Ψ_n, and ω_n (Fig. 1). The remaining angles reflect the local peptide bond geometry. The angle α_{NC_α} denotes the angle between the N–C_α bond and the *y*-axis of the MF corresponding to the *n*th plane, $\alpha_{NC_\alpha} = 151.8°$; γ_{tetra} is the tetrahedral angle, typically 110–112° in

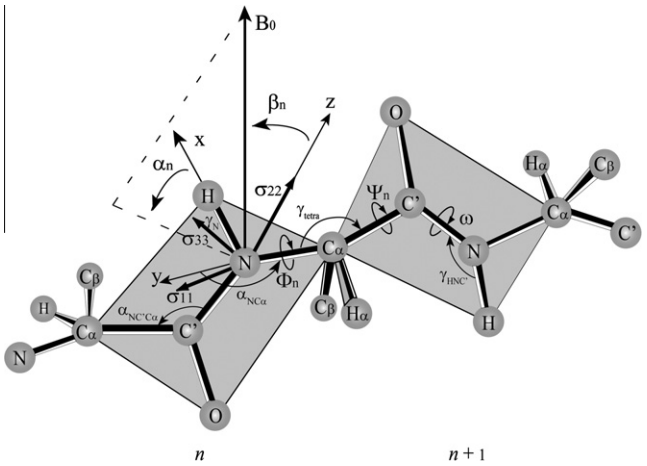

Fig. 1. Local molecular frame associated with a peptide plane. The orientation of the main magnetic field B_0 relative to the *n*th peptide plane is described by two angles α_n and β_n. An approximate orientation of the ^{15}N CSA tensor relative to the peptide plane is represented by arrows originating from the N atom. Two adjacent amino acid residues are linked by the torsion angles Φ_n and Ψ_n. Deviation from peptide planarity is given by the angle ω. The angle α_{NC_α} denotes the angle between the N–C_α bond and the *y*-axis of the MF corresponding to the *n*th plane, γ_N is the angle between the NH bond and the σ_{33} axis of the ^{15}N CSA, γ_{tetra} is the tetrahedral angle, and $\alpha_{NC'C_\alpha}$ and $\gamma_{HNC'}$ are given by the standard peptide plane geometry.

real proteins instead of the ideal value 109.47°. The other angles can be also calculated from the standard peptide plane geometry [41], and are given by: $\alpha_{NC'C_\alpha} = 115.6°$; $\gamma_{HNC'} = 119.5°$. Here, the bond angles are assumed constant for all amino acid residues of the protein.

The orientation of the magnetic field B_0 relative to the MF of the next peptide plane can be calculated in a recursive manner by operating the above propagator matrix $\mathbf{P}(\Phi, \Psi, \omega)$ from the right on the row vector of the spherical harmonics corresponding to the orientation of B_0 with respect to the preceding frame:

$$\vec{\boldsymbol{Y}}(\beta_{n+1}, \alpha_{n+1}) = \vec{\boldsymbol{Y}}(\beta_n, \alpha_n)\mathbf{P}(\Phi_n, \Psi_n, \omega_n) \tag{3}$$

We note that the Wigner rotation matrices in Eq. (2) can be expressed in terms of the angular momentum operators $\mathbf{L}_y$ and $\mathbf{L}_z$ in the following manner [42]:

$$\mathbf{D}(\varphi, \theta, \psi) = e^{-i\varphi\mathbf{L}_z}e^{-i\theta\mathbf{L}_y}e^{-i\psi\mathbf{L}_z} \equiv \mathbf{Z}(-\varphi)\mathbf{Y}(-\theta)\mathbf{Z}(-\psi) \tag{4}$$

Here, the individual angular momentum operators are defined as:

$$\mathbf{L}_x \equiv \frac{1}{\sqrt{2}}\begin{pmatrix} 0 & 1 & 0 \\ 1 & 0 & 1 \\ 0 & 1 & 0 \end{pmatrix}, \quad \mathbf{L}_y \equiv \frac{i}{\sqrt{2}}\begin{pmatrix} 0 & -1 & 0 \\ 1 & 0 & -1 \\ 0 & 1 & 0 \end{pmatrix}, \quad \mathbf{L}_z \equiv \begin{pmatrix} 1 & 0 & 0 \\ 0 & 0 & 0 \\ 0 & 0 & -1 \end{pmatrix} \tag{5}$$

and a short-hand notation is used to designate rotation about the corresponding axis, i.e. $\mathbf{Z}(-\varphi) \equiv \exp(-i\varphi\mathbf{L}_z)$, etc. In the propagator matrix, Eq. (2), the first and the third Euler angles of each Wigner rotation matrix are constant, thus reflecting the highly restrained covalent bond angles, while the second angle (corresponding to a rotation generated by the operator $\mathbf{L}_y$) is variable. However, the non-diagonal form for $\mathbf{L}_y$, Eq. (5), indicates that the number of elements that one needs to calculate is much greater than those required for the diagonal operator, $\mathbf{L}_z$. Consequently, by using the following transformation rules for the rotation operators,

$$\mathbf{X}\left(\frac{\pi}{2}\right)\mathbf{Y}(\theta)\mathbf{X}\left(-\frac{\pi}{2}\right) = \mathbf{Z}(\theta), \quad \mathbf{X}\left(\frac{\pi}{2}\right)\mathbf{Z}(\varphi)\mathbf{X}\left(-\frac{\pi}{2}\right) = \mathbf{Y}(-\varphi) \tag{6}$$

one can diagonalize the variable part for the rotations corresponding to the torsion angles Φ, Ψ, and ω in the propagator, Eq. (2). This is easily accomplished by inserting an extra transformation $\mathbf{T} = \mathbf{X}(\pi/2)$ in the quadratic form, yielding the transformed Q-basis:

$$v = \vec{\mathbf{Q}}(\beta, \alpha)[\mathbf{D}_Q(\Omega_{MP})\mathbf{M}_Q\mathbf{D}_Q^{-1}(\Omega_{MP})]\vec{\mathbf{Q}}^+(\beta, \alpha) \tag{7}$$

Here the spherical harmonics $\vec{\mathbf{Q}}(\beta, \alpha)$ replace $\vec{\boldsymbol{Y}}(\beta, \alpha)$ of Eq. (1) and together with the transformed matrices $\mathbf{D}_Q(\Omega_{MP})$ and $\mathbf{M}_Q$ are given by:

$$\vec{\mathbf{Q}}(\beta, \alpha) = \vec{\boldsymbol{Y}}(\beta, \alpha)\mathbf{T}$$

$$\mathbf{D}_Q(\Omega_{MP}) \equiv \mathbf{T}^{-1}\mathbf{D}(\Omega_{MP})\mathbf{T}, \quad \mathbf{M}_Q \equiv \mathbf{T}^{-1}\mathbf{M}\mathbf{T} \tag{8}$$

For any CSA, the interaction matrix M can be expressed in terms of the principal components σ_{11}, σ_{22} and σ_{33} ($\sigma_{33} > \sigma_{22} > \sigma_{11}$) as:

$$\mathbf{M} = \begin{pmatrix} \frac{\sigma_{11}+\sigma_{22}}{2} & 0 & \frac{\sigma_{22}-\sigma_{11}}{2} \\ 0 & \sigma_{33} & 0 \\ \frac{\sigma_{22}-\sigma_{11}}{2} & 0 & \frac{\sigma_{11}+\sigma_{22}}{2} \end{pmatrix} \tag{9}$$

For instance, for ^{15}N CSA, the corresponding Euler angles are given by: $\Omega_{MP}^{15N} = (\gamma_N, \pi/2, \pi/2 + \alpha_N)$, where $\gamma_N = 15–20°$ is the angle between the NH bond and the σ_{33} axis of the ^{15}N CSA, $\alpha_N = 0–25°$ is the angle between the σ_{22} axis of ^{15}N CSA and the normal of the peptide plane; for ^{1}H CSA, $\Omega_{MP}^{1H} = (-\pi/2, -\pi/2, \pi/2)$. It should be noted, however, that in real polypeptides and proteins, the orientation of the ^{1}H CSA frame is highly variable [28].

For the heteronuclear dipolar couplings, the interaction matrix is the product of the corresponding dipolar coupling constant $\chi \equiv \mu_0\gamma_1\gamma_2 h/16\pi^3 r_{12}^3$ (in Hz) and a diagonal matrix:

$$\mathbf{M} = \chi\begin{pmatrix} -1/2 & 0 & 0 \\ 0 & 1 & 0 \\ 0 & 0 & -1/2 \end{pmatrix} \tag{10}$$

where γ_1 and γ_2 are the gyromagnetic ratios of the two interacting spins, and r_{12} is the interspin distance. For the ^{1}H–^{15}N dipolar couplings, the related Euler angles are given by $\Omega_{MP}^{^1H-^{15}N} = (0, \pi/2, 0)$; for $^{13}C_\alpha$–^{15}N dipolar couplings, the Euler angles for the corresponding transformation are given by $\Omega_{MP}^{^{13}C_\alpha-^{15}N} = (-\alpha_{HNC_\alpha}, \pi/2, 0)$, where $\alpha_{HNC_\alpha} = 118.2°$; for ^{13}C′–^{15}N dipolar couplings, the Euler angles are given by $\Omega_{MP}^{^{13}C'-^{15}N} = (\alpha_{HNC'}, \pi/2, 0)$, where $\alpha_{HNC'} = 119.5°$.

The inclusion of the $^1H_\alpha$–$^{13}C_\alpha$ dipolar couplings, which represent an additional chiral restraint, is necessary to further reduce the number of the orientational solutions. The corresponding transformation associated with the $^1H_\alpha$–$^{13}C_\alpha$ dipolar couplings is given by [19]:

$$\mathbf{D}(\Omega_{MP}^{^1H-^{13}C_\alpha}) = \mathbf{D}(\alpha_{NC_\alpha}, \Phi - \pi/3, \pi/2 - \gamma_{ideal})\mathbf{D}(0, -\pi/2, 0). \tag{11}$$

It should be emphasized that the overall matrix in the square bracket given by Eq. (7) as well as all the non-diagonal rotation matrices need to be calculated only once, and the protein chain geometry is contained in the spherical harmonics $\vec{\mathbf{Q}}(\beta, \alpha)$, which vary throughout the backbone via the new recurrence relation:

$$\vec{\mathbf{Q}}(\beta_{n+1}, \alpha_{n+1}) = \vec{\mathbf{Q}}(\beta_n, \alpha_n)\mathbf{P}_Q(\Phi_n, \Psi_n, \omega_n) \tag{12}$$

where $\mathbf{P}_Q(\Phi, \Psi, \omega) = \mathbf{T}^{-1}\,\mathbf{P}(\Phi, \Psi, \omega)\,\mathbf{T}$.

Eqs. (7)–(12) can be used to determine the torsion angles Φ and Ψ associated with the adjacent residues along the polypeptide backbone iteratively in a sequential manner. Experimental uncertainty can be treated by randomizing the values for the input frequencies within a pre-defined range (in Hz) in order to obtain different structural solutions for each fit within a pre-defined tolerance. The solutions for the torsion angles Φ and Ψ are further restricted by the differential Ramachandran plots [43] to automatically keep only the allowed regions. The normalized Ramachandran plots have been chosen by residue type, and include glycines, prolines, pre-prolines, and the general-type plots [4] as shown in Fig. 2 (with the cutoff for the lowest contour chosen as 10^{-3}). The algorithm [Eqs. (7)–(12)] depicted by the flowchart of Fig. 3 has been programmed in MATLAB (Mathworks, Inc.), and the solutions for the torsion-angles are found by minimizing the difference between the back-calculated frequencies and the simulated NMR data from the known PDB structures. Since the sign of the dipolar interaction cannot be experimentally determined, only absolute values for the dipolar couplings are used. In minimizing the root-mean square (rms) deviations relative to the input frequencies, all CSA and dipolar couplings have been scaled so that their maximum values would correspond to that of the ^{1}H–^{15}N coupling (10 kHz) to achieve equal weight in the fitting. If a pair of Φ and Ψ satisfying the experimental restraints and the pre-defined tolerance (i.e. falling within the "experimental uncertainty", in Hz) is found, the search will proceed to the next pair; otherwise, if no acceptable solution is found, the algorithm will go back several residues (typically 3–5 in the calculations) to search for different solutions. Since MATLAB employs a Simplex-type minimizer (i.e. *fminsearch*), the starting values for the torsion angles are randomized at each residue except those in α-helical regions from −180° to +180° to find possible alternative solutions for every iteration. For residues in the α-helical regions, the torsion angles are sought in the region: $\Phi_0 = -60 \pm 30°$, $\Psi_0 = -45 \pm 30°$. To avoid the algorithm getting stuck at a certain unfavorable

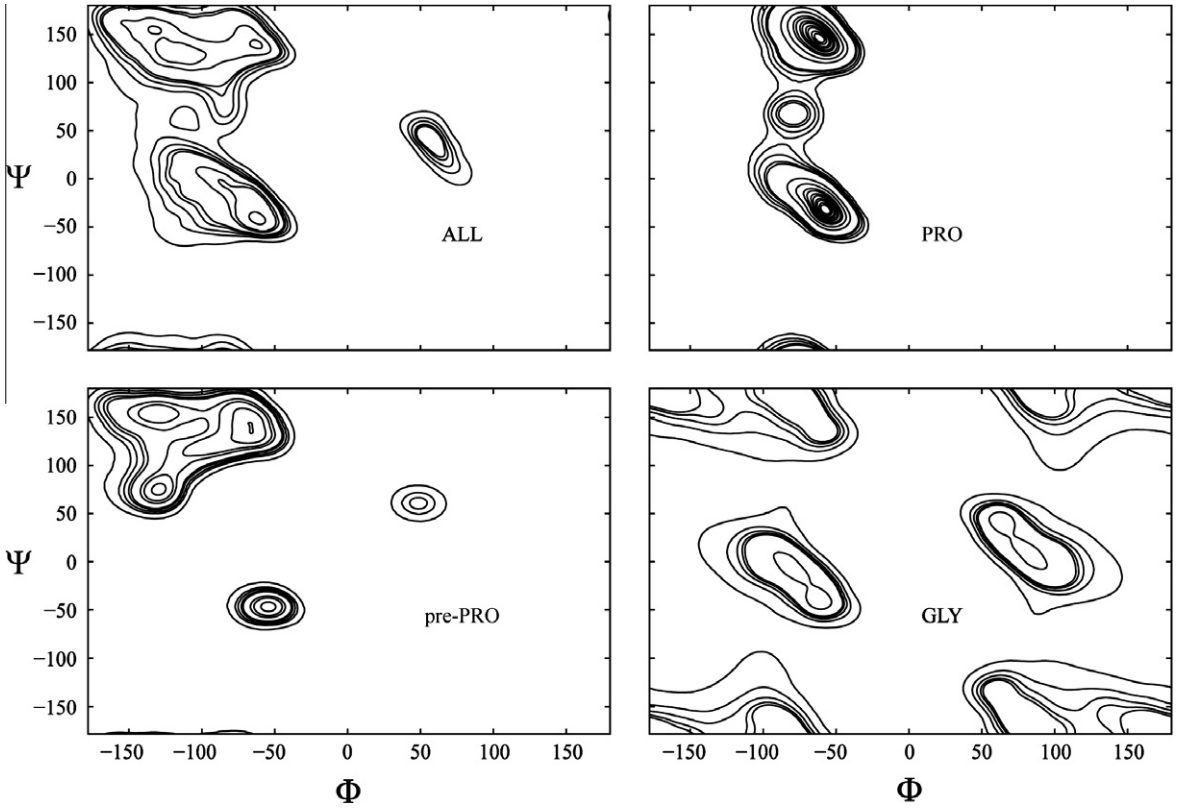

Fig. 2. Normalized Ramachandran plots for different residue types, including glycines, prolines, pre-prolines and the general-type residues with the lowest probability density cutoff of 10^{-3}.

combination of the input data or at a certain residue an automatic restart has been implemented. Any number of frequency constraints can be introduced in the calculations.

3. Results and discussion

3.1. Structural fitting of simulated three-dimensional spectra with ^{15}N CSA, and ^{1}H–^{15}N and ^{1}H–$^{13}C_{\alpha}$ dipolar couplings

Relative convenience of the uniform ^{15}N labeling has rendered two-dimensional solid-state NMR spectra involving ^{15}N CSA and ^{1}H–^{15}N dipolar couplings as a useful tool for the studying of the helical domains of membrane proteins. However, just two spectral dimensions are generally insufficient to calculate tertiary structures of arbitrary topology solely from the oriented-sample NMR data; an important additional angular constraint, the $^{1}H_{\alpha}$–$^{13}C_{\alpha}$ dipolar coupling, needs to be introduced [19]. A simulated three-dimensional solid-state NMR spectrum of protein G (PDB ID 2GB1) is shown in Fig. 4A. When the experimental uncertainty is assumed to be only 0.01 Hz in all dimensions, and no randomization of the input data is performed, back calculation of 100 structures yielded a converged set of solutions as shown in Fig. 4B. The calculated RMSD's relative to the initial structure are about 10^{-5} Å, indicating a mathematically unique solution. Based on the analysis of the structure of protein G (PDB file 2GB1), the torsion angle ω is assumed here to be 178° to describe the deviation from the peptide planarity. The torsion angles Φ and Ψ have been restricted by residue type as described in the previous Section, and Φ and Ψ associated with residues 11 and 37 (our numbering), which correspond to the original residues Glu15 and Gly41, have not been restricted as they would be considered outliers.

However, when just the ^{15}N CSA dimension of the input data is randomly varied within ±1 ppm or ±50 Hz (at 500 MHz ^{1}H NMR frequency), RMSD's of some of the calculated structures become more than 10 Å as shown in Fig. 5. This variation in the CSA was chosen to reflect the above-mentioned uncertainties in both the principal components and, especially, the orientation of the CSA tensor (see Supplementary material for additional simulations). Even a slight randomization of the angle γ_N to within ±1° results in a highly non-uniform variations of the observed ^{15}N CSA frequencies of up to ±3 ppm. To assess the effect of experimental uncertainty in the tensor parameters only, the input data have been simulated by assuming the average tensor values for all amino acids, and the back-calculation has been performed by using the same tensor values. An average uniform ±1 ppm uncertainty was assumed for representative simulations. A two-dimensional projection of the simulated three-dimensional spectra shown in Fig. 5A demonstrates that such small variations in the CSA frequencies (the dots show the fitted values with 100 Hz tolerance) with respect to the original input data (circles) cause a complete scatter in the calculated structures (100 representative structures are shown in Fig. 5B). Such a divergence in the structural solutions is most likely due to the multitude of possible orientational solutions for the weakly restrained torsional conformations in the loop regions that are uniaxially distributed around the magnetic field, as was mentioned in the Introduction.

3.2. Structural fitting of the three-dimensional "shiftless" spectra with ^{1}H–^{15}N, ^{1}H–$^{13}C_{\alpha}$ and $^{13}C_{\alpha}$–^{15}N dipolar couplings

On the other hand, heteronuclear dipolar couplings, which only depend on the covalent bond angles and lengths of the relevant atoms, would seem to represent a much more reliable constraint for the structural fitting than the CSA. The average bond lengths and angles are highly conserved and can be accurately determined [41]. Therefore, the ^{15}N CSA has been replaced by the $^{13}C_{\alpha}$–^{15}N

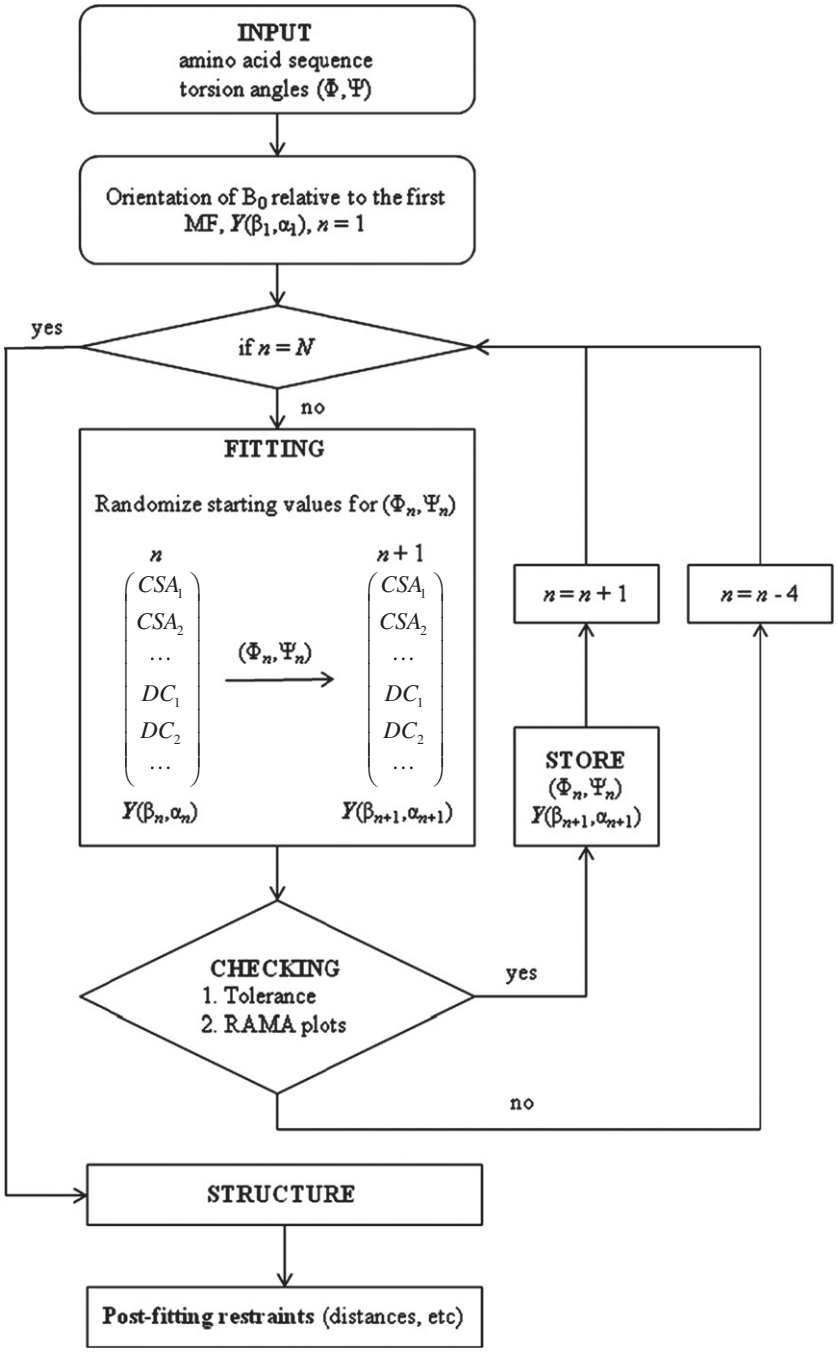

Fig. 3. A flowchart for the structural fitting algorithm. The figure describes the procedure for structure determination by minimizing the difference between the calculated data and the synthetic data generated from the PDB file including the Ramachandran-plot restrictions for the torsion angles Φ and Ψ and post-fitting filtering. Only absolute values for the dipolar couplings are used in the calculations. For further details cf. the text.

dipolar couplings to examine the performance of the "shiftless" [20,21] solid-state NMR data for the structural fitting of protein G. Fig. 4C shows the simulated spectrum. Just as in the case of uniform ^{15}N CSA, a mathematically unique solution as in Fig. 4B can be obtained from the back calculation of the simulated spectra without taking into account any experimental uncertainty. However, when an "experimental uncertainty" of 15 Hz is assumed in all three dimensions, the back-calculated structures begin to diverge (Fig. 6A). More than one half of the RMSDs are around 7 Å. To illustrate the quality of the fit to the synthetic NMR data, we also plot the rms deviations of the fitted frequencies in Hz (over 1000 fits) relative to the "experimental" (i.e. calculated from the PDB coordinates) data for each residue as shown in Fig. 6B. The average rms deviation for all residues is around 7 Hz, and residues 27, 31 (at the ends of the α-helix; our numbering) and 44 (in a β-turn) show somewhat larger deviations.

3.3. Structural fitting of four-dimensional data with ^{1}H–^{15}N, ^{1}H–$^{13}C_{\alpha}$, $^{13}C_{\alpha}$–^{15}N and $^{13}C'$–^{15}N dipolar couplings

An additional dimension, the $^{13}C'$–^{15}N dipolar interaction, has been included to improve the convergence of the calculated structures in the presence of "experimental" uncertainty in the measured couplings. When the data uncertainty is assumed to be 15 Hz, a converged set of solutions containing 1000 structures can be obtained. The structural RMSDs are less than 2 Å as shown

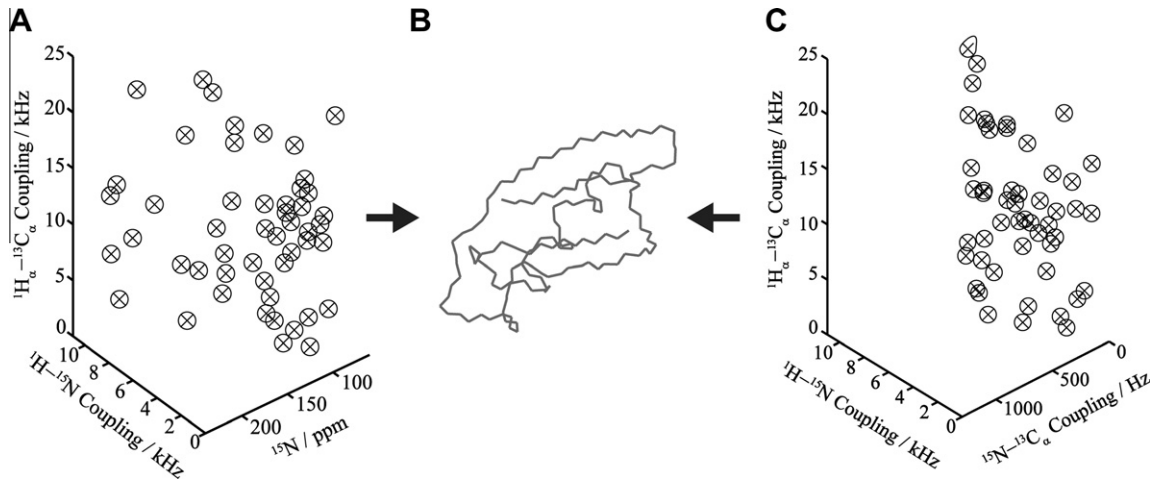

Fig. 4. (A) Structural fitting of the simulated three-dimensional solid-state NMR spectrum of protein G obtained from PDB coordinates 2GB1 including ^{15}N CSA, ^1H–^{15}N dipolar couplings and $^1H_\alpha$–$^{13}C_\alpha$ dipolar couplings. No uncertainty in the input data (circles) is considered. The fitted frequencies are depicted as crosses. (B) A mathematically unique structural solution is obtained that coincides with the original structure. (C) Fitting of simulated three-dimensional "shiftless" solid-state NMR spectra created by substituting the ^{15}N CSA dimension by the $^{13}C_\alpha$–^{15}N dipolar couplings. No experimental uncertainty is assumed. The same unique solution as from fitting the data in part A is obtained.

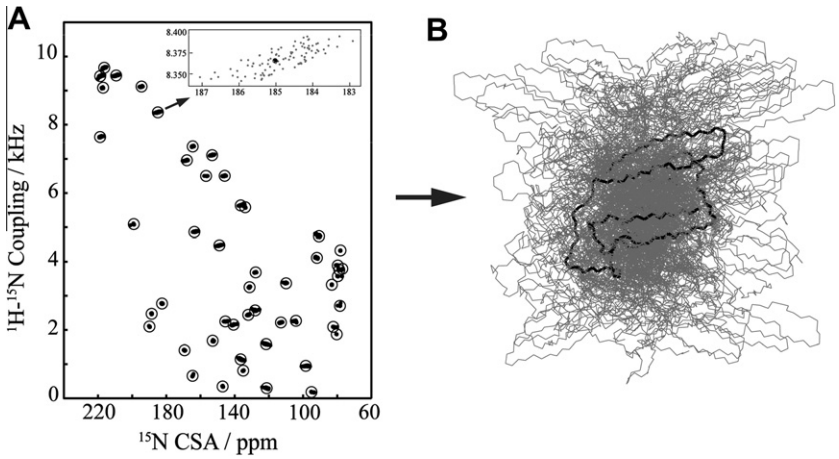

Fig. 5. (A) Two-dimensional projection of the simulated spectra (circles) with the same dimensions as in Fig. 2 with ^{15}N CSA input data randomly varied within 1 ppm for each simulation. The tolerance for the fitting of the input data is 100 Hz. The fitted frequencies are given by dots (no randomization was applied to the other two dimensions). Inset shows a magnified distribution of the fitted frequencies. (B) Back-calculated structures deviate substantially for each simulation. The RMSDs for some of the calculated 100 structures relative to the original structure are more than 10 Å.

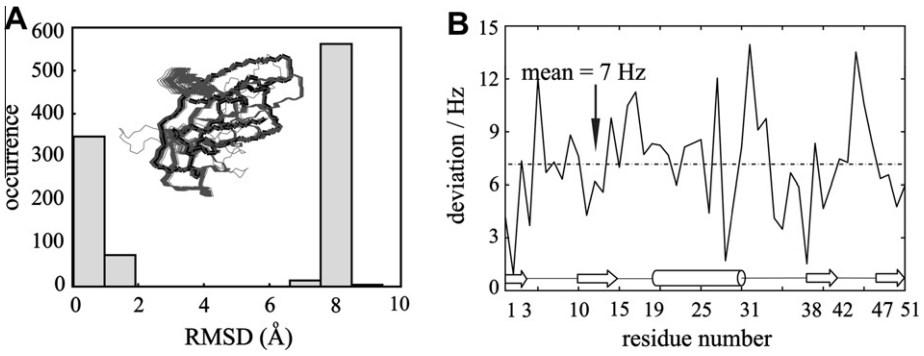

Fig. 6. (A) Structural fitting of simulated three-dimensional "shiftless" solid-state NMR spectra containing ^1H–^{15}N, $^1H_\alpha$–$^{13}C_\alpha$ and $^{13}C_\alpha$–^{15}N dipolar couplings. Histogram of the RMSDs relative to the starting structure shows that when the tolerance for the fitting of the input data is 15 Hz, more than one-half of the RMSDs for 1000 calculated structures are around 7 Å. (B) The root-mean square deviations (in Hz) at each residue for 1000 fits with respect to the synthetic data simulated from the PDB coordinates. The cylinder and the arrows at the bottom represent the α-helix and two β-sheets, respectively.

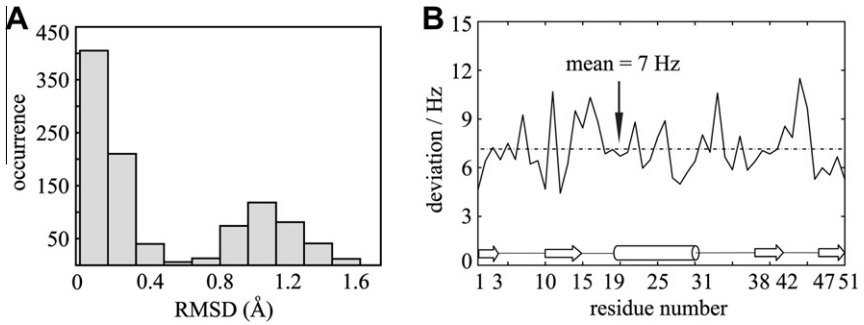

Fig. 7. (A) Structural fitting of simulated four-dimensional data for protein G including additional $^{13}C'$–^{15}N dipolar couplings. With the tolerance for the fitting of the input data of 15 Hz, all back-calculated structures are converged with RMSDs less than 2 Å. (B) The root-mean square deviations (in Hz) at each residue for 1000 fits with respect to the simulated data from the PDB coordinates.

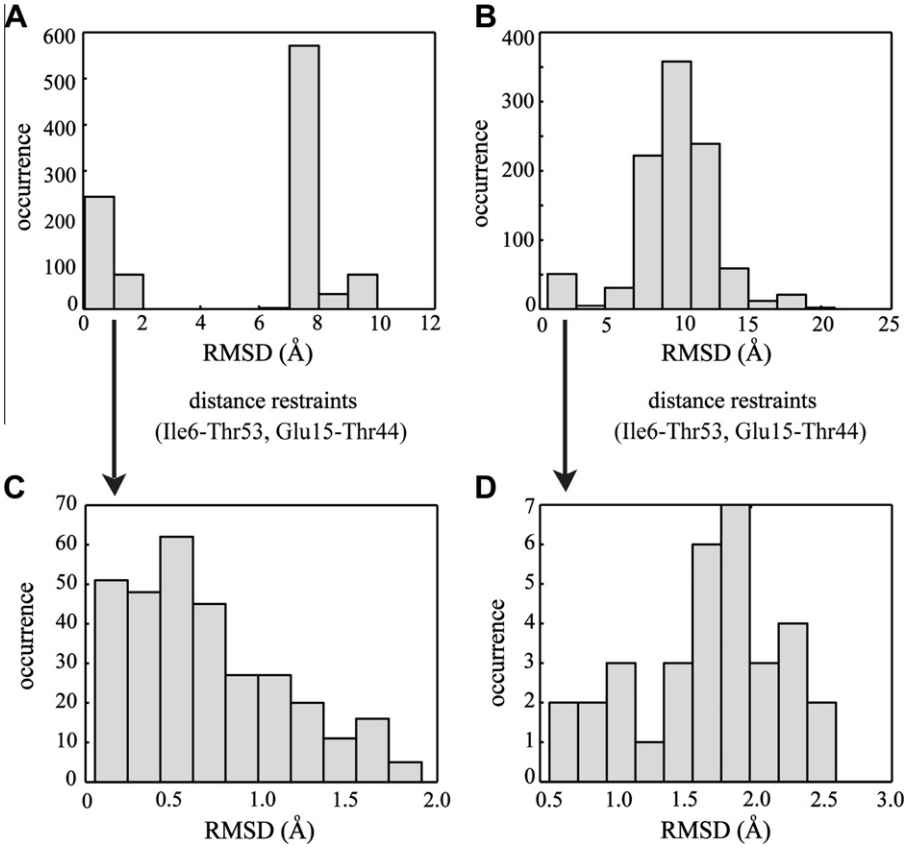

Fig. 8. A and B: Histograms of the RMSDs of 1000 back-calculated structures obtained from three-dimensional "shiftless" solid state NMR spectra of protein G (2GB1) with a tolerance of 25 Hz (A) and 50 Hz (B). C and D: Histograms of the RMSDs for the structures satisfying the distance restraints between the C_α carbons of residues Ile6 and Thr53, and of residues Glu15 and Thr44 for the 25 Hz tolerance (C) and 50 Hz tolerance (D). The inclusion of distance restraints dramatically improves the convergence of the fits with larger tolerances (greater experimental uncertainties).

by the histogram of Fig. 7A. The average deviation of the calculated frequencies from the simulated "experimental' data is around 7 Hz, while residues 11, 16, 33 and 44 (our numbering) are consistently fit less well. The location of residues 16, 33 and 44 is in the β-turn, and residue 11 is at the beginning of a β-sheet, respectively. In OS NMR, the accuracy of the measured dipolar couplings ultimately depends on the stability of the dipolar scaling factor and experimental linewidths (about 200 Hz), so even greater uncertainties may need to be considered. When the tolerance for the fitting of the input data is increased to 25 Hz (and up to 50 Hz) in all four dimensions, the back-calculated structures begin to diverge, and about 40% of the RMSDs are around 7 Å or greater with the average deviation per residue of 12 Hz and higher (see Supplementary material).

Accurate fitting of the residues in the linkage regions or at the beginning/end of an α-helix or β-sheet is important since relatively small deviations at these locations could lead to an entirely different tertiary conformation. Therefore, more information pertaining to the linkage residues may be required to obtain convergent structural solutions for proteins consisting of several secondary structure elements. Specifically, checking for satisfied hydrogen bonds, hydrophobic restraints [44], and electrostatic potential [45] of the entire protein structure within the membrane may be helpful in eliminating the unfavorable solutions [45–47] and treating the

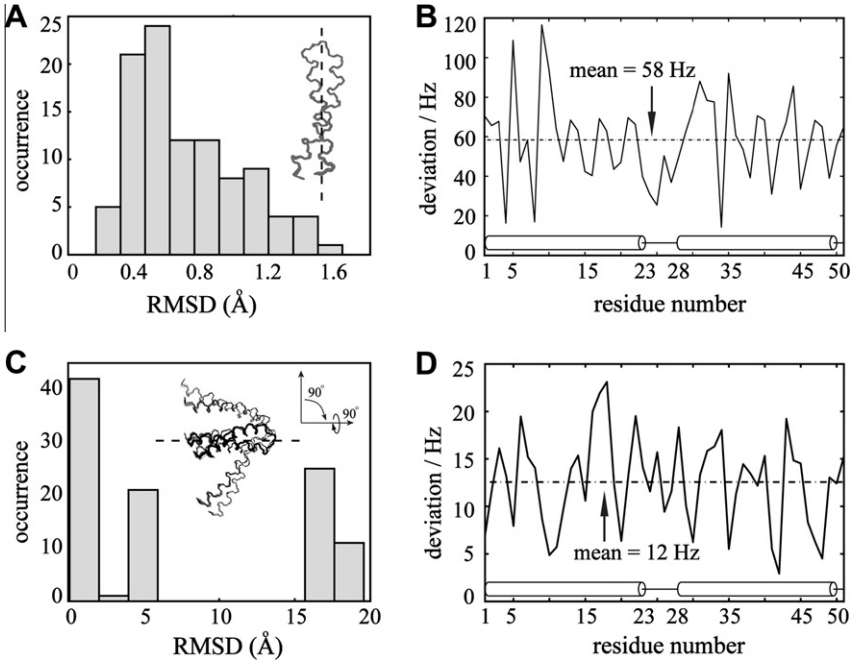

Fig. 9. (A) Structural fitting of simulated three-dimensional "shiftless" spectra of two transmembrane α-helices (residues 104 to 155) of bacteriorhodopsin. When the initial structure is predominantly aligned about the z-axis, with the tolerance for the fitting of the input data of 120 Hz back calculation yields a converged set of solutions having RMSDs of less than 2 Å. (B) The mean of the deviation (in Hz) at each residue for 100 calculated structures with respect to the simulated data from the PDB coordinates. The two cylinders at the bottom depict the α-helices. (C) When the initial structure is rotated by about 90°, with the tolerance of 25 Hz, about 60% of the RMSDs for the back-calculated structures are more than 5 Å. Rotation arrows show the view angles of the calculated structures relative to the original orientation. (D) The rms deviation (in Hz) at each residue for 100 calculated structures shown in part C with respect to the simulated data.

data for the more dynamic loop regions. Moreover, the ab-initio Rosetta method [48], may also be helpful in selecting the plausible backbone conformations by comparing the calculated segments with the known protein structures of similar sequences.

Additional important restraints include long-range distance constraints [44], which are not yet directly accessible in OS NMR but are obtainable from the methyl–methyl NOE data [49] in the liquid state, site-directed spin labeling EPR [50,51] and MAS [52,53]. As an illustrative example, we have calculated structures from the simulated 3D data including the ^{1}H–^{15}N, ^{1}H–$^{13}C_{\alpha}$, and $^{13}C_{\alpha}$–^{15}N dipolar couplings and two distance restraints between the C_{α} atoms of residues Ile6 and Thr53 and residues Glu15 and Thr44 (as determined from the original structure 2GB1; see Supporting Material for additional information). A structure was accepted if both distance restraints were satisfied within ±1 Å. Fig. 8 shows that with a tolerance of 25 Hz, 312 structures (out of 1000 total) satisfying the above distance restraints have the RMSD's of less than 2 Å. When the tolerance is further increased to 50 Hz, 33 out of 1000 back-calculated structures that satisfy the distance restraints have the RMSDs less than 2.5 Å relative to the original structure. Therefore, the number of unfavorable structures can be reduced dramatically by including the distances between two or more pairs of C_{α} atoms as an additional restraint even with larger uncertainties in the input data. The optimal positioning of these restraints depends on the expected protein topology, but longer-distance restraints are generally more stringent [44].

3.4. Structural fitting of a helical hairpin derived from bacteriorhiodopsin

To illustrate the general applicability of the algorithm to other topologies, we have applied it to the simulated data for the light-driven proton pump bacteriorhodopsin, which could be considered as a structural paradigm for G-protein coupled receptors. Bacteriorhodopsin from *Halobacterium salinarum* is composed of seven α-helical transmembrane chains, and was solved by X-ray crystallography with a resolution of 1.55Å [54] (PDB ID 1C3W). Two α-helices (containing residues Asp104-Gly155) have been chosen for a representative calculation. Three-dimensional "shiftless" spectra including ^{1}H–^{15}N, ^{1}H–$^{13}C_{\alpha}$ and $^{13}C_{\alpha}$–^{15}N dipolar couplings have been simulated. The torsion angles have been restricted by the Ramachandran plots having the lowest probability cutoff of 1×10^{-3} for the loop region (residues Leu127-Val130), and within ±30° relative to $\Phi = -60°$, $\Psi = -45°$ for the two helical regions. Interestingly, when the helical hairpin is preferentially aligned about the z-axis (cf. Fig. 9A), which would correspond to its native orientation in the membrane, back-calculation from the synthetic spectrum yields a converged set of solutions with the tolerance up to 120 Hz. (Results with higher tolerances for the input data are presented in the Supplementary material.) By contrast, when the original structure is rotated by 90° (cf. Fig. 9C), the back-calculated structures begin to diverge with a tolerance of only 25 Hz. Fig. 9C shows the top view of the back-calculated structures to illustrate the scatter in the structural solutions. This indicates that error propagates differently into the calculated structures depending on their overall orientation, as expected for inhomogeneously broadened frequency anisotropies. It should be also noted that the analysis using MOLMOL 2.0 [55] of the PDB structure 1C3W has revealed that the twist angle ω for the peptide linkages is around 176°, especially in the connecting loop region. This may imply that deviations from planarity in membrane proteins may need to be treated more differently than for soluble proteins, which exhibit the average value of around 178°. This merits additional investigation as more high-resolution data on membrane proteins become available in the future.

4. Conclusions

We have examined the influence of the variations in the magnitude and orientation of angular-dependent solid-state NMR

observables on the structural fitting of macroscopically aligned proteins. Even though the principal components of the ^{15}N CSA can be determined with high precision, a somewhat undefined orientation of the ^{15}N CSA tensor results in a considerable divergence of the calculated protein structures.

By contrast, multidimensional "shiftless" solid-state NMR spectra involving solely the heteronuclear dipolar couplings associated with the ^{1}H, ^{13}C and ^{15}N spin-bearing nuclei can perform as an efficient tool for the determination of three-dimensional protein structures. This was illustrated by obtaining converged sets of solutions from the synthetic datasets for protein G (a soluble protein) and for bacteriorhodopsin (a transmembrane protein) with a simulated experimental uncertainty of up to 15 Hz and 120 Hz, respectively. Non-planarity of the peptide unit as defined by the third torsion angle, ω has been included in the present version of the algorithm. Moreover, the formulation of the algorithm entirely in the torsion-angle space simultaneously provides both the Ramachandran [56] and C_α-geometry validation [43] "on-a-fly". At present, conformations of transmembrane regions having around 50 residues can be calculated from OS NMR data. With the addition of more constraints, especially those derived from the heteronuclear couplings to ^{13}C spins and long-range distance restraints, "shiftless" solid-state NMR spectra will have the potential of resolving the structures of more complex polypeptides and proteins solely based on the experimental data even in the presence of larger experimental uncertainties.

Acknowledgments

This research is supported by grants MCB 0843520 from NSF and by a Multidisciplinary Research Grant from North Carolina Biotechnology Center.

Appendix A. Supplementary data

Histograms of observable ^{15}N CSA values taking into account variations in the principal components of the CSA tensor (σ_{11}, σ_{22}, σ_{33}) and its orientation as given by the angle γ_N; simulations with larger experimental uncertainty. Supplementary data associated with this article can be found, in the online version, at doi:10.1016/j.jmr.2011.06.008.

References

[1] S.J. Opella, P.L. Stewart, K.G. Valentine, Protein structure by solid-state NMR spectroscopy, Q. Rev. Biophys. 19 (1987) 7–49.
[2] T.A. Cross, S.J. Opella, Solid-state NMR structural studies of peptides and proteins in membranes, Curr. Opin. Struct. Biol. 4 (1994) 574–581.
[3] S.J. Opella, Y. Kim, P. McDonnell, Experimental nuclear magnetic resonance studies of membrane proteins, Methods Enzymol. 239 (1994) 536–560.
[4] A.A. De Angelis, S.C. Howell, A.A. Nevzorov, S.J. Opella, Structure determination of a membrane protein with two trans-membrane helices in aligned phospholipid bicelles by solid-state NMR spectroscopy, J. Am. Chem. Soc. 128 (2006) 12256–12267.
[5] S.J. Opella, A.C. Zeri, S.H. Park, Structure, dynamics, and assembly of filamentous bacteriophages by nuclear magnetic resonance spectroscopy, Annu. Rev. Phys. Chem. 59 (2008) 635–657.
[6] N.J. Traaseth, L. Shi, R. Verardi, D.G. Mullen, G. Barany, G. Veglia, Structure and topology of monomeric phospholamban in lipid membranes determined by a hybrid solution and solid-state NMR approach, Proc. Natl. Acad. Sci. USA 106 (2009) 10165–10170.
[7] M. Sharma, M. Yi, H. Dong, H. Qin, E. Peterson, D.D. Busath, H.-X. Zhou, T.A. Cross, Insight into the mechanism of the influenza A proton channel from a structure in a lipid bilayer, Science 330 (2010) 509–512.
[8] C.H. Wu, A. Ramamoorthy, S.J. Opella, High-resolution heteronuclear dipolar solid-state NMR-spectroscopy, J. Magn. Reson., Ser. A 109 (1994) 270–272.
[9] A. Ramamoorthy, Phase-alternated composite pulses for zero-field NMR spectroscopy of spin 1 systems, Mol. Phys. 93 (1998) 757–766.
[10] B.M. Fung, A.K. Khitrin, K. Ermolaev, An improved broadband decoupling sequence for liquid crystals and solids, J. Magn. Reson. 142 (2000) 97–101.
[11] S.V. Dvinskikh, K. Yamamoto, A. Ramamoorthy, Heteronuclear isotropic mixing separated local field NMR spectroscopy, J. Chem. Phys. 125 (2006) 034507.
[12] A.A. Nevzorov, S.J. Opella, Selective averaging for high-resolution solid-state NMR spectroscopy of aligned samples, J. Magn. Reson. 185 (2007) 59–70.
[13] A.A. De Angelis, S.J. Opella, Bicelle samples for solid-state NMR of membrane proteins, Nat. Protoc. 2 (2007) 2332–2338.
[14] S.H. Park, C. Loudet, F.M. Marassi, E.J. Dufourc, S.J. Opella, Solid-state NMR spectroscopy of a membrane protein in biphenyl phospholipid bicelles with the bilayer normal parallel to the magnetic field, J. Magn. Reson. 193 (2008) 133–138.
[15] S.H. Park, S.J. Opella, Triton X-100 as the "short-chain lipid" improves the magnetic alignment and stability of membrane proteins in phosphatidylcholine bilayers for oriented-sample solid-state NMR spectroscopy, J. Am. Chem. Soc. 132 (2010) 12552–12553.
[16] P.L. Stewart, K.G. Valentine, S.J. Opella, Structural analysis of solid-state NMR measurements of peptides and proteins, J. Magn. Reson. 71 (1987) 45–61.
[17] R. Bertram, T. Asbury, F. Fabiola, J.R. Quine, T.A. Cross, M.S. Chapman, Atomic refinement with correlated solid-state NMR restraints, J. Magn. Reson. 163 (2003) 300–309.
[18] J.K. Denny, J. Wang, T.A. Cross, J.R. Quine, PISEMA powder patterns and PISA wheels, J. Magn. Reson. 152 (2001) 217–226.
[19] A.A. Nevzorov, S.J. Opella, Analytical framework for protein structure determination by solid-state NMR of aligned samples, in: G.A. Webb (Ed.), Handbook of Magnetic Resonance, Kluwer, The Netherlands, 2006.
[20] N. Sinha, C.V. Grant, S.H. Park, J.M. Brown, S.J. Opella, Triple resonance experiments for aligned sample solid-state NMR of ^{13}C and ^{15}N labeled proteins, J. Magn. Reson. 186 (2007) 51–64.
[21] C.H. Wu, S.J. Opella, Shiftless nuclear magnetic resonance spectroscopy, J. Chem. Phys. 128 (2008) 052312.
[22] G.N. Ramachandran, Need for nonplanar peptide units in polypeptide chains, Biopolymers 6 (1968) 1494–1496.
[23] G.N. Ramachandran, A.V. Lakshminarayanan, A.S. Kolaskar, Theory of the non-planar peptide unit, Biochim. Biophys. Acta 303 (1973) 8–13.
[24] M.W. MacArthur, J.M. Thornton, Deviations from planarity of the peptide bond in peptides and proteins, J. Mol. Biol. 264 (1996) 1180–1195.
[25] S. Scheiner, C.W. Kern, Theoretical studies of environmental effects on protein conformation. 1. Flexibility of the peptide bond, J. Am. Chem. Soc. 99 (1977) 7042–7050.
[26] T.G. Oas, C.J. Hartzell, F.W. Dahlquist, G.P. Drobny, The amide ^{15}N chemical shift tensors of four peptides determined from ^{13}C dipole-coupled chemical shift powder patterns, J. Am. Chem. Soc. 109 (1987) 5962–5966.
[27] C.J. Hartzell, M. Whitfield, T.G. Oas, G.P. Drobny, Determination of the ^{15}N and ^{13}C chemical shift tensors of L-[^{13}C]Alanyl-L-[^{15}N]alanine from the dipole-coupled powder patterns, J. Am. Chem. Soc. 109 (1987) 5966–5969.
[28] G. Cornilescu, A. Bax, Measurement of proton, nitrogen, and carbonyl chemical shielding anisotropies in a protein dissolved in a dilute liquid crystalline phase, J. Am. Chem. Soc. 122 (2000) 10143–10154.
[29] A.E. Walling, R.E. Pargas, A.C. de Dios, Chemical shift tensors in peptides: a quantum mechanical study, J. Phys. Chem. A 101 (1997) 7299–7303.
[30] D.K. Lee, J.S. Santos, A. Ramamoorthy, Nitrogen-15 chemical shift anisotropy and ^{1}H–^{15}N dipolar coupling tensors associated with the phenylalanine residue in the solid state, Chem. Phys. Lett. 309 (1999) 209–214.
[31] D.K. Lee, R.J. Wittebort, A. Ramamoorthy, Characterization of ^{15}N Chemical Shift and ^{1}H-^{15}N dipolar coupling interactions in a peptide bond of uniaxially oriented and polycrystalline samples by one-dimensional dipolar chemical shift solid-State NMR spectroscopy, J. Am. Chem. Soc. 120 (1998) 8868–8874.
[32] J. Herzfeld, A.E. Berger, Sideband intensities in NMR spectra of samples spinning at the magic angle, J. Chem. Phys. 73 (1980) 6021–6030.
[33] W.T. Franks, D.H. Zhou, B.J. Wylie, B.G. Money, D.T. Graesser, H.L. Frericks, G. Sahota, C.M. Rienstra, Magic-angle spinning solid-state NMR spectroscopy of the *b* 1 Immunoglobulin Binding Domain of Protein G (GB1): ^{15}N and ^{13}C chemical shift assignments and conformational analysis, J. Am. Chem. Soc. 127 (2005) 12291–12305.
[34] B.J. Wylie, L.J. Sperling, H.L. Frericks, G.J. Shah, W.T. Franks, C.M. Rienstra, Chemical-shift anisotropy measurements of amide and carbonyl resonances in a microcrystalline protein with slow magic-angle spinning NMR spectroscopy, J. Am. Chem. Soc. 129 (2007) 5318–5319.
[35] K. Loth, P. Pelupessy, G. Bodenhausen, Chemical shift anisotropy tensors of carbonyl, nitrogen, and amide proton nuclei in proteins through cross-correlated relaxation in NMR spectroscopy, J. Am. Chem. Soc. 127 (2005) 6062–6068.
[36] C.H. Wu, A. Ramamoorthy, L.M. Gierasch, S.J. Opella, Simultaneous characterization of the amide ^{1}H chemical shift, ^{1}H–^{15}N dipolar, and ^{15}N chemical shift interaction tensors in a peptide bond by three-dimensional solid-state NMR spectroscopy, J. Am. Chem. Soc. 117 (1995) 6148–6149.
[37] A.A. Nevzorov, S.J. Opella, Structural fitting of PISEMA spectra of aligned proteins, J. Mag. Reson. 160 (2003) 33–39.
[38] F.M. Marassi, S.J. Opella, A solid-state NMR index of helical membrane protein structure and topology, J. Magn. Reson. 144 (2000) 150–155.
[39] F.M. Marassi, S.J. Opella, Using Pisa pies to resolve ambiguities in angular constraints from PISEMA spectra of aligned proteins, J. Biomol. NMR 23 (2002) 239–242.
[40] R.C. Page, S. Kim, T.A. Cross, Transmembrane helix uniformity examined by spectral mapping of torsion angles, Structure 16 (2008) 787–797.

[41] R.A. Engh, R. Huber, Accurate bond and angle parameters for X-ray protein structure refinement, Acta. Cryst. A47 (1991) 392–400.
[42] G.B. Arfken, Mathematical Methods for Physicists, third ed., Academic Press, Orlando, 1985.
[43] S.C. Lovell, I.W. Davis, W.B. Arendall III, P.I.W. de Bakker, J.M. Word, M.G. Prisant, J.S. Richardson, D.C. Richardson, Structure validation by Cα geometry: ϕ,ψ, and Cβ deviation, Proteins: Struct., Funct., Genet. 50 (2003) 437–450.
[44] D.M. Standley, V.A. Eyrich, A.K. Felts, R.A. Friesner, A.E. McDermott, A branch and bound algorithm for protein structure refinement from sparse NMR data sets, J. Mol. Biol. 285 (1999) 1691–1710.
[45] F. Dong, B. Olsen, N.A. Baker, Computational methods for biomolecular electrostatics, Methods Cell Biol. 84 (2008) 843–870.
[46] W. Im, M. Feig, C.L. Brooks III, An implicit membrane generalized born theory for the study of structure, stability, and interactions of membrane proteins, Biophys. J. 85 (2003) 2900–2918.
[47] L. Shi, N.J. Traaseth, R. Verardi, A. Cembran, J. Gao, G. Veglia, A refinement protocol to determine structure, topology and depth of insertion of membrane proteins using hybrid solution and solid-state NMR restraints, J. Biomol. NMR 44 (2009) 195–205.
[48] R. Bonneau, J. Tsai, I. Ruczinski, D. Chivian, C. Rohl, C.E.M. Strauss, D. Baker, Rosetta in CASP4: progress in Ab initio protein structure prediction, Proteins: Struct., Funct., Genet. 5 (2001) 119–126.
[49] K.H. Gardner, M.K. Rosen, L.E. Kay, Global folds of highly deuterated, methyl-protonated proteins by multidimensional NMR, Biochemistry 36 (1997) 1389–1401.
[50] P.P. Borbat, J.H. Freed, Multiple-quantum ESR and distance measurements, Chem. Phys. Lett. 313 (1999) 145–154.
[51] C. Altenbach, A.K. Kusnetzow, O.P. Ernst, K.P. Hofmann, W.L. Hubbell, High-resolution distance mapping in rhodopsin reveals the pattern of helix movement due to activation, PNAS 105 (2008) 7439–7444.
[52] C.P. Jaroniec, B.A. Tounge, J. Herzfeld, R.G. Griffin, Frequency selective heteronuclear dipolar recoupling in rotating solids: accurate ^{13}C–^{15}N distance measurements in uniformly ^{13}C,^{15}N-labeled peptides, J. Am. Chem. Soc. 123 (2001) 3507–3519.
[53] W. Luo, R. Mani, M. Hong, Side-chain conformation of the M2 transmembrane peptide proton channel of influenza A virus from ^{19}F solid-state NMR, J. Phys. Chem. B 111 (2007) 10825–10832.
[54] H. Luecke, B. Schobert, H.-T. Richter, J.-P. Cartailler, J.K. Lanyi, Structure of bacteriorhodopsin at 1.55 Angstrom resolution, J. Mol. Biol. 291 (1999) 899–911.
[55] R. Koradi, M. Billeter, K. Wuthrich, MOLMOL: a program for display and analysis of macromolecular structures, J. Mol. Graphics 14 (1996) 51–55.
[56] R.A. Laskowski, PROCHECK: a program to check the stereochemical quality of protein structures, J. Appl. Crystallogr. 26 (1993) 283–291.